# Quantum detector tomography applied to the human visual system: a feasibility study

Reep, T.H.A. van der; Molenaar, D.; Löffler, W.; Pinto, Y.

Research Article Vol. 40, No. 2 / February 2023 / Journal of the Optical Society of America A 285

Journal of the Optical Society of America A

OPTICS, IMAGE SCIENCE, AND VISION

# Quantum detector tomography applied to the human visual system: a feasibility study

T. H. A. VAN DER REEP,[1,2,*] D. MOLENAAR,[1] W. LÖFFLER,[2] AND Y. PINTO[1]

[1]Psychology Research Institute, Nieuwe Achtergracht 129b, 1018 WS Amsterdam, The Netherlands
[2]Leiden Institute of Physics, Niels Bohrweg 2, 2333 CA Leiden, The Netherlands
*Corresponding author: t.h.a.vanderreep@uva.nl

Received 13 October 2022; revised 2 December 2022; accepted 15 December 2022; posted 16 December 2022; published 13 January 2023

**We show that quantum detector tomography can be applied to the human visual system to explore human perception of photon number states. In detector tomography, instead of using very hard-to-produce photon number states, the response of a detector to light pulses with known photon statistics of varying intensity is recorded, and a model is fitted to the experimental outcomes, thereby inferring the detector's photon number state response. Generally, light pulses containing a Poisson-distributed number of photons are utilized, which are very easy to produce in the lab. This technique has not been explored to study the human visual system before because it usually requires a very large number of repetitions not suitable for experiments on humans. Yet, in the present study we show that detector tomography is feasible for human experiments. Assuming a simple model for this accuracy, the results of our simulations show that detector tomography is able to reconstruct the model using Bayesian inference with as few as 5000 trials. We then optimize the experimental parameters in order to maximize the probability of showing that the single-photon accuracy is above chance. As such, our study opens the road to study human perception on the quantum level.** 

https://doi.org/10.1364/JOSAA.477639

## 1. INTRODUCTION

With the advancement of quantum optics, detectors have been developed that are sensitive to single photons. However, determining *how* sensitive the detectors are to $n$-photon number states is a nontrivial problem, since a light source producing photon number states is not available. This difficulty has been overcome by quantum detector tomography techniques [1–3], in which the detector's "clicking" probability is inferred by irradiating it with light pulses that are readily available, such as pulses with Poissonian photon statistics from a laser.

A similar case can be made for the detection of light by the human visual system: How well can humans perceive few-photon states? The challenge for detecting such states is to overcome the intrinsic noise in the visual system. To our knowledge, this is the first time a quantum technique such as detector tomography is considered for studying human perception, although it has been proposed to use quantum biometry as a secure identification process [4]. Since the 1940s, it has been known from experiments by Hecht *et al.* that the human visual system is sensitive to light pulses containing only a few photons [5]. In later experiments, similar and lower limits have been found, down to the single-photon level [6,7]. Recently, Tinsley *et al.* presented evidence that humans are indeed able to detect single photons with an accuracy above chance [8]. This is quite remarkable, given that the overall efficiency of the human eye, from cornea up to producing a retinal signal, is only $0.1 - 0.4$ [9–11], and a single photon will trigger a single rhodopsin molecule only [4], which has to be amplified and read out in the noisy environment of the brain. Knowing the limits of human visual perception informs us about the boundaries of the perceptual machinery. This, in turn, is fundamental for our understanding of how the brain generates conscious perception. For instance, to enable conscious awareness of just one photon, specific signal-to-noise mechanisms (e.g., without broad averaging) seem required.

In their analysis, Hecht *et al.* assumed a step function: $n$-photon states are either imperceivable ($n < n_{\mathrm{crit}}$) or fully perceivable ($n \geq n_{\mathrm{crit}}$), whereas Tinsley *et al.* only considered the perceptibility of single photons. In the present study, we will consider detector tomography as a solution to bridge the gap between these two approaches and determine the perceptibility of few-photon states. Apart from this, we can use the techniques to optimize our experimental design, i.e., using our proposed technique, we determine the experimental parameters necessary to statistically demonstrate above-chance performance in a single-photon perception task. We implement our technique in a Bayesian modeling framework, which has a number of advantages over a frequentist approach (see e.g., [12]). For the present study, the most important reason to rely on Bayesian statistics is that it allows quantification of all relevant hypotheses (i.e., the null-hypothesis of chance performance and the alternative hypothesis of above-chance performance). Using frequentist

significance tests, it is only possible to quantify evidence against the null-hypothesis such that the null-hypothesis can never be confirmed. Note that despite this advantage of Bayesian statistics over frequentist statistics, a Bayesian approach to hypothesis testing has not been applied to detector tomography yet.

Our setting is the following: we consider a single test subject that performs a two-alternative forced choice (2AFC) task (see Section 2). During the trials, Poisson-distributed few-photon states are sent to the subject's eye in one of two possible intervals. The subject has to indicate from which interval the pulse was sent, from which the accuracy can be determined. We assume that the pulses have a wavelength of 500 nm, at which the quantum efficiency of the rods in the retina is maximal. The pulses are sent towards the location on the retina where rods are most abundant (16°−23° away from the yellow spot [8,13,14]).

The difficulty of this setting lies in the fact that the repetition rate of the experiment is low. Where detector tomography for, e.g., avalanche photodiodes or superconducting photodetectors can be collected at a rate in the range kilohertz to megahertz, respectively [1,3], typical repetition rates for human test subjects are 0.1−1 Hz [8,14]. Human subjects have a limited attention span, which further decreases the data collection rate (data collection sessions can last for presumably ∼2 h maximally). This implies we would like to measure at a low average photon number only, whereas ordinarily detector tomography is applied to measurements at average photon numbers ranging from imperceivable to always perceivable.

In this work, we show that detector tomography is feasible with a human test subject by simulating the proposed experiment. Apart from that, we determine the optimal experimental parameters for excluding imperceptibility of single photons, given that single photons can be perceived by (modeled) humans with an accuracy above the chance level. First, we explain 2AFC tasks and detector tomography with Poissonian light pulses. In Section 4, we develop a simple visual perception model describing the $n$-photon accuracies, since to our knowledge such a model has not been considered yet. Section 5 describes the computer simulation, after which we dive into reconstruction (parameter recovery) of the model from our simulation data. Here we apply detector tomography in the framework of Bayesian inference. In Section 6, we show that the reconstruction returns $n$-photon accuracy values in agreement with our model. We continue by determining the optimal experimental parameters for excluding imperceptibility of single photons in Section 7. In this section, we also determine the influence of our visual detection model and the influence of noise on the average photon number emitted by the light source. We discuss our results and extensions to our simulation and reconstruction programs in Section 8, after which we conclude in Section 9.

## 2. TWO-ALTERNATIVE FORCED CHOICE TASKS

In psychophysics, the quantitative study of relations between physical and psychological events, 2AFC tasks are often employed as a technique to determine the limits of perception [15,16]. Intuitively, the probability $P$ of perceiving a weak light pulse can be determined in a series of trials, in which randomly the pulse is presented or not; see Fig. 1(a). For each trial, subjects are asked whether a pulse was present or not, which is referred to as a yes/no task in psychophysics.

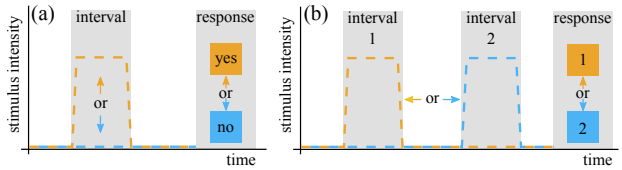


**Fig. 1.** Schematic overview of (a) a yes/no task and (b) a (time separated) 2AFC task. In a yes/no trial, a stimulus is either present or absent in a single interval, and the subject indicates whether a stimulus is detected. In a 2AFC trial, a stimulus is presented in one of two intervals, and a test subject indicates in which interval the stimulus was presented.

This contrasts with the 2AFC task measuring a subject's accuracy $A$ of perceiving the pulse of light. In every trial of such tasks, subjects are presented with a pulse in one of two intervals, whereas in the other interval no pulse is presented; see Fig. 1(b). The interval in which the stimulus is presented is chosen randomly, each with probability of 1/2. These intervals can be separated in space (did the stimulus come from left or right?) or in time (was the stimulus presented early or late? This is also referred to as a two-interval forced choice (2IFC) task). After a 2AFC trial, the subjects are forced to select the interval in which they believe the actual light pulse was presented.

$P$ and $A$ are—in theory—related as

$$A = \frac{1}{2}(1 + P). \tag{1}$$

The lower limit of $A$ of 1/2 arises because if subjects do not detect the stimulus, a random guess has to be made in which interval the stimulus was presented. An accuracy in excess of 1/2 implies the test subject is able to detect the stimulus with a nonzero probability. Finally, if subjects always detect a stimulus, $A$ and $P$ both equal 1.

In practice, however, Eq. (1) does not hold necessarily. Yes/no tasks are more susceptible to response bias. The decision threshold to answer "yes" in such experiments is left free to the subjects, who may choose to rate the various trials anywhere in the range from strict to loose. Subjects may even alter their decision threshold (un)willingly, which greatly influences the experimental data; see e.g., [7]. Alternatively, in 2AFC tasks, subjects rate the difference in sensory input between the two intervals, tackling this issue. Although 2AFC experiments are influenced by interval bias, the influence of this bias can be minimized [17,18]. For this reason we will consider a 2AFC task in this study.

## 3. DETECTOR TOMOGRAPHY WITH POISSONIAN LIGHT PULSES

Detector tomography can be used to obtain the $n$-photon accuracy of a test subject for a range of $n$-photon states, while not possessing a source producing these states deterministically. Instead, one uses a source for which the photon-number distribution is known and uses statistics to infer the $n$-photon accuracies. Hence, let us consider a light source with a known photon-number distribution. i.e., we know the probability that

the source presents $n = 0, 1, 2, \ldots$ photons to the subject. In such a case, the accuracy for some constant source setting with known photon-number distribution is given by [3] (Note that a similar equation would arise for a yes/no task in an experiment measuring detection probability, in which the subject merely notes whether a light pulse was observed.)

$$\begin{aligned} A(I_s) &= \sum_{n=0}^{\infty} a_n \rho_n(I_s) \\ &= 1 - \sum_{n=0}^{\infty} (1 - a_n)\rho_n(I_s) \\ &\approx 1 - \sum_{n=0}^{n_{\max}} (1 - a_n)\rho_n(I_s). \end{aligned} \tag{2}$$

In this equation, $I_s$ are the parameters that determine the photon-number distribution of the source, $a_n$ is the accuracy of the subject for *exactly* $n$ photons, and $\rho_n(I_s)$ is the probability that the source with settings $I_s$ emits $n$ photons. We rewrite this equation in the second line straightforwardly to terminate the sum in practice: When a stimulus with $n_{\max} + 1$ photons is always detected ($a_{n_{\max}+1} = 1$) or when the experiment is designed such that trials with $n_{\max} + 1$ photons are practically not present, whereas trials with $n = 0, \ldots, n_{\max}$ do occur ($\rho_{0,\ldots,n_{\max}} > 0$, $\rho_{n_{\max}+1} \approx 0$), the sum terminates. This is stipulated in the third line of the equation, which introduces the parameter $n_{\max}$ explicitly.

For Poissonian light sources, the photon-number distribution is determined by

$$\rho_n = \exp(-\bar{N})\frac{\bar{N}^n}{n!}. \tag{3}$$

Here, $\bar{N}$ is the average number of photons per light pulse. Substituting Eq. (3) into Eq. (2), we arrive at an accuracy for mean photon number $\bar{N}$ of

$$A(\bar{N}) = 1 - \exp(-\bar{N}) \sum_{n=0}^{n_{\max}} (1 - a_n)\frac{\bar{N}^n}{n!}. \tag{4}$$

In a 2AFC task, $A(I_s)$ is measured and $\rho_n(I_s)$ is known for several $I_s$. This allows one to reconstruct $\vec{a} = [a_0, a_1, \ldots, a_{n_{\max}}]$ by fitting Eq. (2) to the measured data. For light pulses with Poissonian photon statistics, one would fit Eq. (4), of course. Finding $\vec{a}$ and $n_{\max}$ is the goal of detector tomography, a process which is further described in Section 5.

## 4. VISUAL PERCEPTION MODEL

The model describing the subject's accuracy (for constant source setting) $A$, given the source's photon number distribution $\rho_n$ presented in Eq. (2), depends heavily on the $n$-photon accuracies $a_n$. Of course, $a_0 = 0.5$ due to a lack of photons being presented to the subject and [8] estimates $a_1 \approx 0.516$. To our knowledge, however, no experimental bounds have been obtained for $a_{>1}$. Thus, in order to perform the feasibility study, which is the main topic of this study, we need to construct a model for $\vec{a}$: the visual perception model.

In order to construct the model, let us consider a Gaussian pulse of $n$ photons with a wavelength of 500 nm. If such a pulse is focused on the retina, these photons land on the retina within an area of approximately $S = \pi w_0^2$, where the beam waist,

$$w_0 = \frac{\lambda}{\pi n_{\text{eye}}\theta} \approx 3\ \mu\text{m}. \tag{5}$$

In this equation, $n_{\text{eye}} \approx 1.337$ is the refractive index of the eye and $\theta$ is the convergence angle of the pulse. If the pulse of collimated light is focused by a lens with a 2 cm-radius and a focus distance of 50 cm, $\theta \approx 4 \times 10^{-2}$ rad. This implies $S \approx 3 \times 10^1\ \mu\text{m}^2$. From [13], we estimate that a single rod cell covers approximately 5 $\mu\text{m}^2$ of retinal area, implying the pulse covers approximately six rod cells.

If, on the other hand, a Maxwellian view [19] is used during the experiments, in which the pulse is focused on the eye lens (instead of the retina) and a small area of the retina is irradiated, $S \approx \pi(d_{\text{eye}}\theta/n_{\text{eye}})^2 \approx 1.(6) \times 10^6\ \mu\text{m}^2$, assuming the diameter of the eye equals 24 mm. In this case, the pulse covers approximately $3 \times 10^5$ rod cells.

We intend to use the Maxwellian view during our experiments, which maximizes the number of photons from the pulse entering the eye. Additionally, focusing the pulse on the eye lens prevents this lens from influencing the path of the photons, such that we do not need to take precautions fixating the focal distance of the eye. Given that we will consider approximately 10 photons per pulse at most, the calculation presented before implies that in this case, it is likely that all photons reach a different rod. If we furthermore assume that at such light levels all rods function independently, we are led to a binomial model for $a_n$, i.e., we set a single photon detection probability, $p_1$, and calculate

$$p_n = 1 - (1 - p_1)^n. \tag{6}$$

From this equation,

$$a_n = \frac{1}{2}(1 + p_n), \tag{7}$$

similar to Eq. (1), which is the final necessity to simulate an experiment. We note that the reconstruction method that will be discussed in Section 5 does not depend on the model we constructed for $a_n$.

## 5. SIMULATION AND RECONSTRUCTION

To simulate the envisioned experiment, we have written a simulation program in R [20]. In this program, we set the minimum and maximum intensity $\bar{N}_{\min}$ and $\bar{N}_{\max}$, which range is divided in $D$ equidistant data points. Together these are the $\vec{\bar{N}}$ intensities for the Poissonian light source. Additionally, we set the number of trials per data point $d$, $T$, and the noise of the light source. We consider the following noise model:

$$\bar{N}_d = \bar{N}_{d,0} + \mathrm{d}\bar{N}_d, \tag{8}$$

where $\mathrm{d}\bar{N}_d \sim \mathcal{N}(0, \sigma_{\bar{N},d})$, i.e., for all trials, we add a normally distributed random deviation (0-mean, $\sigma_{\bar{N},d}$-standard deviation) to the intended mean photon number $\bar{N}_{d,0}$. For each of the

data points, we calculate the theoretical accuracy by setting the single-photon detection probability $p_1$ and using Eqs. (6), (7), and (4).

As a next step, we simulate the trials. For each trial for each data point $d$ (at source intensity $\bar{N}_{d,0}$), we draw a source intensity deviation $\mathrm{d}\bar{N}_d$. Sequentially, we draw $n$ photons from a Poisson distribution with mean photon number $\bar{N}_d$. $n$ represents the number of photons presented to the subject's eye. Assuming the subject to be unbiased and performing Bernoulli trials, we draw the trial outcome from a Bernoulli distribution with accuracy $a_n$; see Eq. (7). This results in either a correct or a wrong response. We sum the number of correct responses per data point and thus obtain a one-dimensional array of length $D$, which elements are the number of correct responses for data point $d$ at mean photon number $\bar{N}_{d,0}$. This array we will refer to as $\vec{\Sigma}$.

Using the data array with trial outcomes, our goal is to obtain $n_{\max}$ and reconstruct the model accuracies $\vec{a} = [a_0, a_1, \ldots, a_{n_{\max}}]$ set by the user. Here we give a summary of the methods. The interested reader may refer to Supplement 1, Section S1 for a more elaborate discussion.

For a given $n_{\max}$, we perform the reconstruction of $\vec{a}$ under Bayesian inference using a program written in RStan [21]. The program takes $\vec{\Sigma}$ as input. Apart from this array, the number of data points $D$, the number of trials per data point $T$, $n_{\max}$, and the $\boldsymbol{\rho}$-matrix need to be specified. The latter is a $D \times (n_{\max}+1)$-matrix whose indices are given by $\boldsymbol{\rho}_{d,n} = \exp(-\bar{N}_d)\bar{N}_d^n/n!$, i.e., $\boldsymbol{\rho}$ contains the theoretical probabilities for presenting $n = 0, \ldots, n_{\max}$ photons.

Using this program, we obtain parameter estimates for $\vec{a}$ by Markov chain Monte Carlo (MCMC) sampling from the posterior distribution of these unknown parameters,

$$p(\vec{\tilde{a}}|\vec{\Sigma}) \propto p(\vec{\Sigma}|T, \vec{\tilde{a}})\, p(\vec{\tilde{a}}), \tag{9}$$

and taking the posterior mode of these samples. The resulting Markov chains (MCs) of samples from the posterior distribution have a length,

$$N_{\mathrm{MC}} = \frac{N_{\mathrm{chains}}\left(N_{\mathrm{iter}} - N_{\mathrm{warmup}}\right)}{N_{\mathrm{thin}}}, \tag{10}$$

where $N_{\mathrm{chains}}$ is the number of parallel chains evaluated (in this study typically 3), $N_{\mathrm{iter}}$ is the number of iterations (in this study typically 15,000), $N_{\mathrm{warmup}}$ is the number of initial iterations discarded to ensure convergence of the sampling algorithm (in this study typically 2500), and $N_{\mathrm{thin}}$ is the amount of thinning in the chain decrease in the autocorrelations among the samples (in this study typically 3).

In Eq. (9), $\vec{\tilde{a}}$ is the reconstruction of $\vec{a}$. $p(\vec{\tilde{a}})$ is the prior distribution of $\vec{\tilde{a}}$ [which we will denote as $p(\vec{\tilde{a}}^{(0)})$ from now on] and $p(\vec{\Sigma}|T, \vec{\tilde{a}})$ is the likelihood of the data $\vec{\Sigma}$ given $T$ and $\vec{\tilde{a}}$. For the posterior $p(\vec{\tilde{a}}|\vec{\Sigma})$ we will use the shorthand notation $p(\vec{\tilde{a}}^{(1)})$. Below we discuss the prior distribution and likelihood in more detail. This technical description is added here for completeness, but readers may skip ahead to Section 6.

For $p(\vec{\tilde{a}}^{(0)})$, we choose a prior distribution determined by a beta($\alpha$, $\beta$)-distribution with hyper-prior shape parameters,

$$\alpha \sim \mathrm{halfnorm}\left(1,\ 1/2 + n_{\max}/2 - n_{\max}^2/35\right), \tag{11}$$

$$\beta \sim \mathrm{halfnorm}\left(1,\ 12 - n_{\max}/1.8 - n_{\max}^2/200\right). \tag{12}$$

As discussed in Supplement 1, Section S1.1, the beta($\alpha$, $\beta$)-distribution for specific $\alpha$ and $\beta$ can be seen as a prior model for the detection probability $\vec{\tilde{p}} = 2\vec{\tilde{a}} - 1$ [Eq. (7)]. By drawing sets of $n_{\max}$ samples from the prior beta-distribution, where each set is sorted and appended to 0 (thus yielding the drawn prior vector $\vec{\tilde{p}}^{(0)} = [0, \tilde{p}_1^{(0)}, \ldots, \tilde{p}_{n_{\max}}^{(0)}]$ ($\tilde{p}_n^{(0)} < \tilde{p}_{n+1}^{(0)}$ due to sorting)) and finally transformed as $\vec{\tilde{a}}^{(0)} = (1 + \vec{\tilde{p}}^{(0)})/2$, we find that the distribution $p(\vec{\tilde{a}}^{(0)})$ complies with our common sense and current knowledge of $\vec{a}$ (see Supplement 1, Section S1.1): $\tilde{a}_0^{(0)} = 1/2$ (0 photons are imperceivable), $\tilde{a}_n^{(0)} < \tilde{a}_{n+1}^{(0)}$ (the $n$-photon accuracy rises with number of photons), $p(\tilde{a}_1^{(0)})$ peaks between $\tilde{a}_n^{(0)} = 0.5$ and 0.6 as found by [8], whereas $p(\tilde{a}_{>1}^{(0)})$ is broader due to our lack of knowledge about these accuracies. The $n_{\max}$-contribution to the hyper-priors in Eq. (11) ensures that the distribution $p(\vec{\tilde{a}}^{(0)})$ is constant, irrespective of the value of $n_{\max}$. For the posterior, we use the same transformations as described for the prior; hence, $\tilde{a}_0^{(1)} = 1/2$ and $\tilde{a}_n^{(1)} < \tilde{a}_{n+1}^{(1)}$, as required by common sense.

To determine the likelihood of $\vec{\Sigma}$ given $\vec{\tilde{a}}$, we use the binomial distribution,

$$p\left(\vec{\Sigma}|T, \vec{\tilde{a}}\right) = \prod_{d=1}^{D} \binom{T}{\Sigma_d} \tilde{A}_d^{\Sigma_d} (1 - \tilde{A}_d)^{T - \Sigma_d}, \tag{13}$$

where $\vec{\tilde{A}} = \vec{1} - \boldsymbol{\rho}(\vec{1} - \vec{\tilde{a}})$; see Eq. (4).

In order to determine $n_{\max}$, we must show that $\tilde{a}_{n_{\max}+1}$ is irrelevant for the reconstruction, hence, that $p(\tilde{a}_{n_{\max}+1}^{(0)}) = p(\tilde{a}_{n_{\max}+1}^{(1)})$—the prior equals the posterior; see Supplement 1, Section S1.2 for further details. The determination of $n_{\max}$ starts with a reconstruction at a value of $n_{\max}$ too low (typically $\bar{N}_{\max} + 1$). We add $\tilde{p}_{n_{\max}+1}^{(0)}$ to $\vec{\tilde{p}}^{(0)}$ and multiplex the reconstruction, i.e., we perform the reconstruction $N_{\mathrm{mult}}$ times in parallel by mapping $\vec{\tilde{p}}^{(0)} \mapsto \tilde{\boldsymbol{p}}^{(0)}$, a matrix of dimensions $(n_{\max}+2) \times N_{\mathrm{mult}}$. Accordingly, the vectors $\vec{\tilde{a}}^{(0)}$ and $\vec{\tilde{A}}^{(0)}$ are mapped to matrices $\tilde{\boldsymbol{a}}^{(0)}$ and $\tilde{\boldsymbol{A}}^{(0)}$ with dimensions $(n_{\max}+2) \times N_{\mathrm{mult}}$ and $D \times N_{\mathrm{mult}}$, respectively. The $\boldsymbol{\rho}$-matrix is augmented to size $D \times (n_{\max}+2)$ to incorporate the probability of sending $n_{\max}+1$ photons.

The likelihood of the data $\vec{\Sigma}$ is evaluated separately for each of the multiplexes. For $\tilde{p}_{n_{\max}+1}$, we set a beta(2.5, 0.5)-prior, which we transform to the domain $[p_{\min}, 1]$, such that $\tilde{p}_{n_{\max}+1}^{(0)} > \tilde{p}_{n_{\max}}^{(0)}$ is likely. Initially, upon starting the $n_{\max}$ determination, we set $p_{\min} = 0$. We compare the $N_{\mathrm{mult}}$ MCs of $\tilde{p}_{n_{\max}+1}^{(0)}$ and $\tilde{p}_{n_{\max}+1}^{(1)}$, based on which we decide whether $n_{\max}$ is set to a sufficiently high value (i.e., $p(\tilde{p}_{n_{\max}+1}^{(0)})$ and $p(\tilde{p}_{n_{\max}+1}^{(1)})$ are indiscernible). In case we find that $n_{\max}$ is insufficient, we increase the value by 1 and update the value of $p_{\min}$ as described in Supplement 1, Section S1.2. Then we perform the multiplexed reconstruction again until a sufficient value for $n_{\max}$ has been determined.

The RStan-program returns MCs for all matrix elements of $\tilde{\boldsymbol{a}}^{(0)}$, $\tilde{\boldsymbol{a}}^{(1)}$, and $\tilde{\boldsymbol{A}}^{(1)}$. However, because $\tilde{\boldsymbol{a}}^{(1)}$ is the multiplexed version of $\vec{\tilde{a}}^{(1)}$ and all multiplexes have been compared to the same data, the MCs for all multiplexes can be appended together, i.e., we can "squeeze" the columns of $\tilde{\boldsymbol{a}}^{(0)}$, $\tilde{\boldsymbol{a}}^{(1)}$, and $\tilde{\boldsymbol{A}}^{(1)}$ back to $\vec{\tilde{a}}^{(0)}$, $\vec{\tilde{a}}^{(1)}$, and $\vec{\tilde{A}}^{(1)}$, such that the MC for each $\tilde{a}_n^{(0)}$, $\tilde{a}_n^{(1)}$, or $\tilde{A}_d$ contains $N_{\text{mult}} \cdot N_{\text{MC}}$ samples.

From the latter MCs, we can determine the posterior statistics, such as means, medians, modes, and high-density intervals (HDIs) using the DBDA2E-utility.R-functions provided by [22].

An example of the posterior statistics of $\vec{\tilde{a}}^{(1)}$ and $\vec{\tilde{A}}^{(1)}$ is discussed in the next section.

## 6. SINGLE SIMULATION AND RECONSTRUCTION RESULT

Let us perform a single simulation as described in the previous section. We set $N_{\text{min}} = 1.0$, $\bar{N}_{\text{max}} = 3.0$, and $D = 5$ such that $\vec{\bar{N}} = [1.0, 1.5, 2.0, 2.5, 3.0]$, and $\sigma_{\bar{N},d} = 0$ (no noise). For each data point we perform $T = 1000$ trials, i.e., we run a total of 5000 trials equally divided over 5 data points. For the reconstruction, we set $N_{\text{mult}} = 7$, $N_{\text{chains}} = 3$, $N_{\text{iter}} = 15000$, $N_{\text{warmup}} = 2500$, and $N_{\text{thin}} = 3$. This yields $N_{\text{MC}} = 12500$ per multiplex and therefore 87,500 MCMC samples per $\tilde{a}_n^{(1)}$ in total.

The reconstruction for the constant source accuracy $\vec{A}$, $\vec{\tilde{A}}^{(1)}$ is shown in Fig. 2. Here, we plot the reconstructed values of the experimental outcome $A_d^{\text{MLE}} = \Sigma_d / T$ with yellow asterisks. Indicated HDIs for each $\tilde{A}_d^{(1)}$ are spanned by blue lines, whereas the posterior modes of $\vec{\tilde{A}}^{(1)}$ are marked with a red dot, giving an impression of the posterior distribution. As can be observed, the reconstructed values are close to the model values, which we obtain by direct substitution of the $n$-photon accuracies $\vec{a}$ [Eqs. (11) and (7)] into Eq. (4). This is a direct result from the detector tomography technique we apply.

In Fig. 3, the reconstructed values for $\vec{a}$, $\vec{\tilde{a}}^{(1)}$, can be observed, obtained from the same simulation. The posterior distributions corresponding to each $\tilde{a}_n^{(1)}$ are indicated in the same fashion as for $\tilde{A}_d^{(1)}$. We find good agreement between $\vec{a}$ and $\vec{\tilde{a}}^{(1)}$. Comparing Fig. 3 to Fig. 2, we see that $\vec{\tilde{a}}^{(1)}$ "follows" $\vec{\tilde{A}}^{(1)}$, as one should expect. Low (high) values for $A_d^{\text{MLE}}$ drags (lifts) $\vec{\tilde{a}}^{(1)}$ down (up).

From this reconstruction, we can determine whether single photons are detected ($\tilde{a}_1^{(1)} > 0.5$). To this end, we estimate the Savage–Dickey ratio [23],

$$r_{\text{SD}}(0.5) = 10 \log_{10}\left(\frac{p(\tilde{a}_1^{(1)} = 0.5)}{p(\tilde{a}_1^{(0)} = 0.5)}\right). \tag{14}$$

This ratio allows us to exclude a value of 0.5 for $\tilde{a}_1^{(1)}$ if the posterior drops significantly below the prior, i.e., in our case, a *decreasing* $r_{\text{SD}}(0.5)$ indicates *increasing* evidence that a single photon can indeed be detected. Although other decision criteria are available (see, e.g., [24]), we choose to evaluate the Savage-Dickey ratio here because of its ease in interpretation.

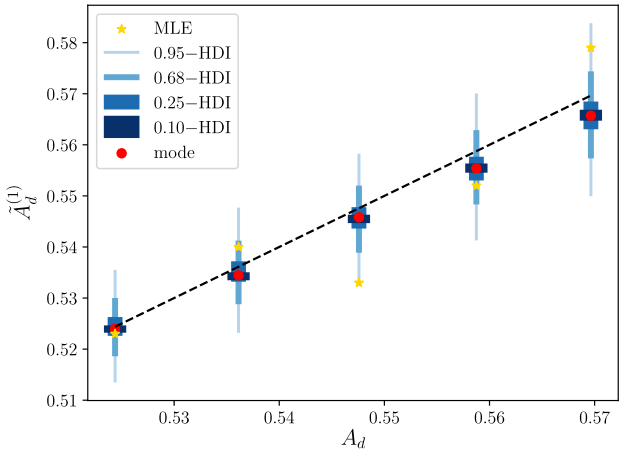


**Fig. 2.** Reconstruction of the accuracy per data point (source intensity) for a single simulation. $\vec{A}$ are the model values obtained from substituting our model for $\vec{a}$ [Eqs. (6) and (7)] into Eq. (4). The black dashed line indicates $\tilde{A}_d^{(1)} = A_d$ to guide the eye. Although the most likely accuracy values ($A_d^{\text{MLE}} = \Sigma_d / T$, yellow asterisks) are different from the model values, the reconstruction $\vec{\tilde{A}}^{(1)}$ (indicated by specified HDIs and the mode) is closer to the model values as a result of the detector tomography techniques we apply.

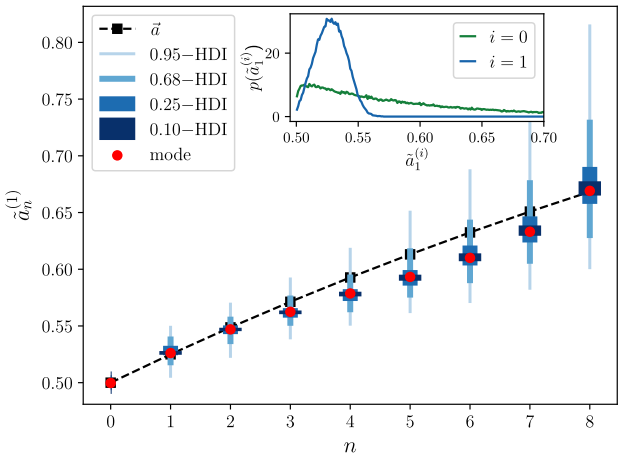


**Fig. 3.** Reconstruction of the accuracy for $n$-photon states for a single simulation. The posterior distributions of $\tilde{a}_n^{(1)}$ are indicated using specified HDIs and the distribution mode. The black dashed line corresponds to our model values. The inset shows the prior and posterior distributions for $\tilde{a}_1$. From this figure one may estimate the Savage–Dickey ratio (see text), $r_{\text{SD}}$, at $\tilde{a}_1 = 0.5$ as an indicator whether the data exclude $\tilde{a}_1^{(1)} = 0.5$ (a single photon is undetected). For this simulation $r_{\text{SD}}(0.5) = -4.9$.

The prior and posterior distributions $p(\tilde{a}_1^{(0)})$ and $p(\tilde{a}_1^{(1)})$ for the simulation under consideration in this section have been depicted in the inset of Fig. 3. Fitting these distributions with a logspline-function from the logspline-library [25] available for R gives us an estimate for $r_{\text{SD}}(0.5)$. For this simulation, we found $r_{\text{SD}}(0.5) = -4.9$ dB, which is on the verge of being considered substantial evidence that single photons can be detected [26].

We can also estimate how well the higher-photon number accuracies are reconstructed. For this purpose, we calculate the

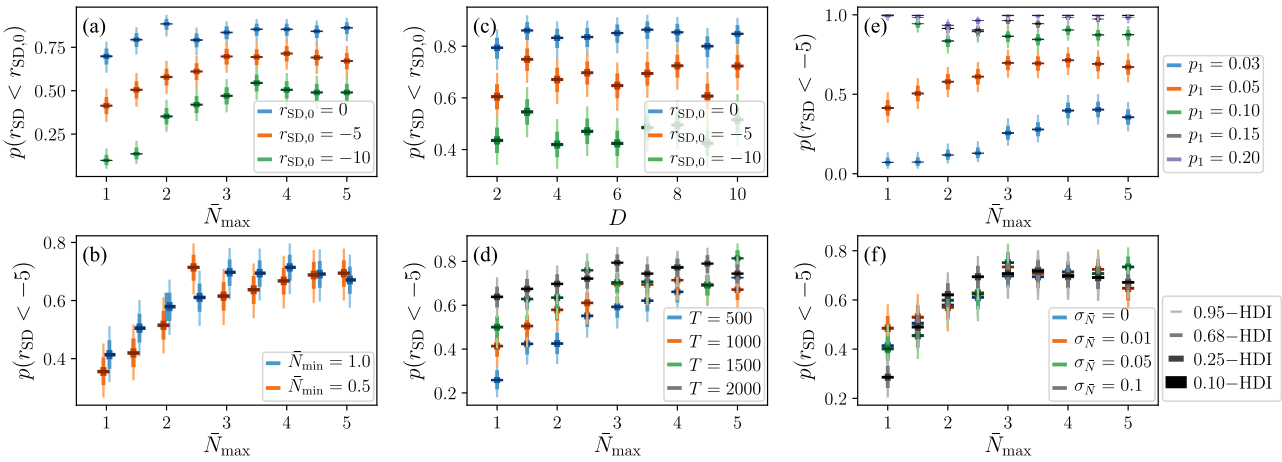


**Fig. 4.** Experimental success probability based on the Savage–Dickey ratio, $p(r_{SD}(0.5) < r_{SD,0})$, under variation of experimental and model parameters. (a) Experimental success probability as a function of $\bar{N}_{max}$ ($\bar{N}_{min} = 1.0$, $T = 1000$, $D = 5$, $p_1 = 0.05$, and $\sigma_{\bar{N},d} = 0$); MCMC parameters as stated in text; the success probability rises linearly for low $\bar{N}_{max}$ and becomes constant for $\bar{N}_{max} > 3$, irrespective of the cut-off ratio chosen for marking a successful experiment. (b) The value for $\bar{N}_{min}$ is of minor importance. For $\bar{N}_{min} = 1.0$ and 0.5, respectively, [other parameters equal to the values in (a)], the maximum experimental success probability is hardly influenced by $\bar{N}_{min}$. The data are offset by ±0.05 in their $\bar{N}_{max}$-value for clarity. (c) Varying $D$ while keeping $D \cdot T$ constant at 5000 trials shows that $D$ is also of minor importance [$\bar{N}_{max} = 3.0$—other parameters as stated under (a)]; (d) influence of the total number of trials by varying $T$ [other parameters as in (a)]; it is observed that the slope in the experimental success probability for $\bar{N}_{max} < 3.0$ decreases, while its constant value increases slightly with $T$. (e) Variation in the visual model value $p_1$ [all other parameters equal to those in (a)] reveals that the value of $\bar{N}_{max}$ for which the experimental success probability becomes constant decreases with $p_1$. (f) The reconstruction is resilient to noise in the light source. Varying $\sigma_{\bar{N}}$ [other parameters the same as in (a)], it is observed that the experimental success probability does not vary, except for $\bar{N}_{max} = 1.0$. Based on these results, the optimal experimental parameters seem to be $\bar{N}_{min} = 1.0$, $\bar{N}_{max} = 4.0$, $D \geq 3$, and $D \cdot T \geq 5000$, while noise in the light source is not detrimental to the experiment.

mean of squared errors of mode($\vec{\tilde{a}}^{(1)}$) relative to $\vec{a}$,

$$\mathrm{MSE}(a_n) = \frac{1}{n_{max}} \sum_n \left(\mathrm{mode}(\tilde{a}_n^{(1)}) - a_n\right)^2. \quad \textbf{(15)}$$

For the reconstruction result presented in Figs. 2 and 3, this calculation evaluates to $1.66 \times 10^{-4}$, implying the reconstructed mode is 1.29% off on average for the eight reconstructed accuracies.

## 7. OPTIMIZATION OF EXPERIMENTAL PARAMETERS FOR SINGLE-PHOTON DETECTION

Using the simulation and reconstruction algorithm, we can optimize the experimental parameters $\vec{\bar{N}}$, $D$, and $T$ in order to achieve a certain goal. Apart from that, we study the influence of the model parameters $p_1$ and $\sigma_{\bar{N},d}$. Being interested in whether single photons are detected, we consider the Savage-Dickey ratio in this section and estimate the experimental success probability $p(r_{SD}(0.5) < r_{SD,0})$, where $r_{SD,0}$ is the threshold value below which we consider $\tilde{a}_1^{(1)} = 0.5$ excluded. In Supplement 1, Section S2, we consider some other optimization goals.

$p(r_{SD}(0.5) < r_{SD,0})$ is estimated by performing 100 simulations for given experimental parameters and calculating the Savage-Dickey ratio for each. Since these simulations can be considered as binomial trials, in which $r_{SD}(0.5) < r_{SD,0}$ implies success, we determine the uncertainty in the success probability by setting a beta(1, 1)-prior (flat prior) for this parameter. Then, the posterior is a beta($k + 1$, $100 + 1$)-distribution, where $k$ is the number of simulations for which $r_{SD}(0.5) < r_{SD,0}$.

Our optimization results are presented in Fig. 4. For $\bar{N}_{max}$ we consider values up to 5.0, for which $\rho_1$, Eq. (3), has decreased to only 3.4%. On the other hand, since $\rho_1$ maximizes for $\bar{N} = 1$, we consider this value as a maximum for $\bar{N}_{min}$.

In general, we observe that the experimental success probability shows two regimes. For lower $\bar{N}_{max}$, the success probability is seen to rise linearly, whereas above a critical $\bar{N}_{max,c}$, it remains constant. This behavior is apparent under variation of all other experimental and model parameters (except $D$), and $r_{SD,0}$. As can be seen in Fig. 4(a), in which we plotted the success probability for $\bar{N}_{min} = 1.0$, $p_1 = 0.05$, $D = 5$, $T = 1000$ and a noiseless source, $\bar{N}_{max,c} \approx 3.0$ does not depend on $r_{SD,0}$. Taking $r_{SD,0} = -5$, it is seen that $p(r_{SD}(0.5) < r_{SD,0})$ rises to approximately 0.7. It rises more or less to the same value if we set $\bar{N}_{min} = 0.5$, as can be observed in Fig. 4(b). It reaches this value for slightly higher $\bar{N}_{max}$, and in general the success probability seems to be lower for $\bar{N}_{min} = 0.5$ than for $\bar{N}_{min} = 1.0$, except for $\bar{N}_{max} = 2.5$. We attribute these results to the fact that $\rho_1$ maximizes for $\bar{N} = 1$, such that for any $\vec{\bar{N}}$ that contains $\bar{N} = 1$, sending one photon is most likely. Therefore, we infer that $\bar{N}_{min} = 1$ will be optimal for our experiments.

In Fig. 4(c), we plot our results for varying $D$, while keeping $D \cdot T = 5000$ ($\bar{N}_{min} = 1.0$, $\bar{N}_{max} = 3.0$; other parameters the same). Thus, it is clearly observed that it does not matter whether we perform many trials on a few source intensities, or rather a few trials for many source intensities. This can be understood since the number of trials per photon number is more or less constant for every combination of $D$ and $T$ if $D \cdot T$ is kept constant. However, it should be noted that if one optimizes for the smallest $\tilde{a}_1^{(1)}$ 0.95-HDI, which is performed

in Supplement 1, Section S2, $D \geq 3$ is a better choice. Hence, we would still advise performing the experiment at least three source intensities.

The final experimental parameter we consider is the total number of trials $D \cdot T$. As can be seen in Fig. 4(d), $\bar{N}_{\mathrm{max,c}}$ does not vary with $D \cdot T$ [setting $D = 5$, other parameters as in Fig. 4(a)]. However, with increasing $D \cdot T$, the slope at $\bar{N}_{\max} < \bar{N}_{\mathrm{max,c}}$ decreases and the constant value that the success probability attains increases. The latter increase, however, is only small, from which it follows that 5000 trials ($T = 1000$) is sufficient for the experiment.

Apart from the experimental parameters, we also study the influence of the model parameters $p_1$ and $\sigma_{\bar{N},d}$. In Fig. 4(e), we plot our results for the experimental success probability while varying $p_1$ [other parameters the same as stated for Fig. 4(a)]. $p_1 = 0.03$ and $p_1 = 0.20$ correspond to the accuracies reported by [8] averaged over all trials and high-confidence trials, respectively. It is clearly observed that the success probability drops while decreasing $p_1$. This is, of course, due to $a_1$ becoming closer to 0.5, such that a difference from 0.5 is harder to detect. Interestingly, we also observe that $\bar{N}_{\mathrm{max,c}}$ increases with decreasing $p_1$. Based on this observation, we would advise setting $\bar{N}_{\max}$ to 4.0 during the actual experiment because the actual value for $p_1$ not well known.

Finally, we study the influence of noise on the light source. We set $\sigma_{\bar{N},d}$ to a constant $\sigma_{\bar{N}}$. Although such a model ($\sigma_{\bar{N},d}$ constant for all data points) would only be valid for light sources that are linear, we expect that this simple model reveals the most important aspects of a noisy light source. We observe in Fig. 4(f) that the influence of noise on the experiment is minor. Only for $\bar{N}_{\min} = \bar{N}_{\max} = 1.0$ does noise seem to be of negative influence to the success probability. We suspect that this mainly results from the photon number distribution being fairly constant under influence of our noise model. This follows from the Taylor expansion of $\rho_n$,

$$\begin{aligned}\rho_n &= \exp\left(-\left(\bar{N}_{d,0} + \mathrm{d}\bar{N}\right)\right) \frac{\left(\bar{N}_{d,0} + \mathrm{d}\bar{N}\right)^n}{n!} \\ &= \exp\left(-\bar{N}_{d,0}\right) \frac{\bar{N}_{d,0}^n}{n!} \\ &\times \left[1 - \left(1 - \tfrac{n}{\bar{N}_{d,0}}\right) \mathrm{d}\bar{N} + \left(\tfrac{1}{2} - \tfrac{n}{\bar{N}_{d,0}} + \frac{\binom{n}{2}}{\bar{N}_{d,0}^2}\right) \mathrm{d}\bar{N}^2 - \ldots\right] \\ &\approx \exp\left(-\bar{N}_{d,0}\right) \tfrac{\bar{N}_{d,0}^n}{n!} \left[1 - \left(1 - \tfrac{n}{\bar{N}_{d,0}}\right) \mathrm{d}\bar{N}\right]. \end{aligned} \tag{16}$$

Upon direct comparison of the first and last line of this equation, we find that the approximation holds for $\mathrm{d}\bar{N} < 0.15\bar{N}_{d,0}$. Since the approximation is linear in $\mathrm{d}\bar{N}$, the photon number distribution remains more or less constant for any distribution $\mathrm{d}\bar{N}$ symmetric around 0. From this argument, we expect that noise on $\bar{N}_{d,0}$ yields no problem for the experiment as long as its distribution is symmetric and the standard deviation of $\bar{N}_d$ is less than $0.05\bar{N}_{d,0}$.

In summary, from our results we find that the experimental success probability for detecting that $\tilde{a}_1^{(1)} > 0.5$ is optimized for setting $\bar{N}_{\min} = 1.0$, $\bar{N}_{\max} = 4.0$, $D \geq 3$, and $D \cdot T \geq 5000$. The standard deviation of the noise on the light source should be less than $0.05\bar{N}_{d,0}$.

## 8. DISCUSSION

Throughout this study, we have made several assumptions that influence the experiments that will be discussed below. Also, we will compare our approach of using a light source with a Poissonian photon number distribution to a source based on spontaneous parametric downconversion (SPDC), as used by [8]. Finally, we will describe how the data collected in the proposed experiment can also be used to determine the $n$-photon accuracies referenced to the retina.

Since this is the first time that the method of detector tomography has been considered for the human visual system, it was necessary to construct a model for $\vec{a}$. Under the assumption that the eye receptors function independently effectively, they receive at most one photon per light pulse and their quantum efficiency remains constant in time, we proposed a binomial model. Using a Maxwellian view, in which the light pulse is spread over a relatively large area of the retina (order $10^5$ receptors), it is likely that each receptor receives at most one photon. However, since visual signal processing is highly nonlinear, we doubt that the assumption on effective independence of receptors can be made, even at this scale. Moreover, from [8] it is known that it is more likely to detect single photons if the time between single-photon events decreases. This implies the quantum efficiency of the receptors is not constant in reality. These points are even more valid for the case in which the light pulse is focused on the retina, implying only order 10 receptors partake in receiving the photons. In this case, one also cannot make the assumption any more that each photons lands on a different receptor. These effects can be studied experimentally by shifting the focal point of the light pulses between the eye lens and the retina and varying the time in between trials. Additionally, the irradiated part of the retina can be adapted by changing the focal distance of the focusing lens (the $f = 50$ cm-lens discussed in Section 4). This would allow us to study summation effects [14,27] in the visual system with few-photon number states.

We overcome the lack of knowledge on $\vec{a}$ by defining a prior that can take into account many models for $\vec{a}$, not one specific for our model. However, since we assume $\tilde{a}_{n+1} > \tilde{a}_n$, models for which $\tilde{a}_{n+1} \leq \tilde{a}_n$ are excluded. Also, although the amount of possible models that can be described using our prior is broad, not all possible models can be described. Therefore it remains a question about whether a more suitable prior can be found.

Our other major assumption is that the test subject performs Bernoulli trials. In reality, however, $\vec{a}$ for a subject may vary in time (intersession and intrasession) due to, e.g., fluctuations in the quantum efficiency of the receptors (as already discussed), tiredness, or other fluctuations in attention [28]. Therefore, a beta-binomial likelihood, in which $\vec{a}$ is allowed to vary in between trials, might be more suitable. If the experiment shows that this is the case, RStan does allow to implement the beta-binomial likelihood easily. However, performing the reconstruction based on the binomial likelihood will return the mean $\tilde{\vec{a}}^{(1)}$, even if the beta-binomial likelihood proves to be more suitable. Another suggestion would be to perform the reconstruction with a hierarchical Bayesian model, in which the data is fitted per session and which also returns a hyper-$\tilde{\vec{a}}^{(1)}$ for the subject.

The same holds when considering different test subjects together. Because everyone's visual system is different, one would expect that for every subject $\vec{a}$ differs as well. If the data of all subjects are pooled together, one would find the mean $\vec{\tilde{a}}^{(1)}$ for these subjects. Upon writing a hierarchical model, however, one would obtain information about each subject individually. It would even be possible to add two hierarchical layers, one intersubject and another one intersession.

If hierarchy is added to the reconstruction, the amount of trials rises accordingly, i.e., in case data of all participants is pooled, 5000 trials is sufficient to obtain an estimate of their mean $\vec{\tilde{a}}^{(1)}$. When intertest subject differences are taken into account, this number rises to 5000 trials per participant, which is still a feasible number of trials. For studying intratest subject effects, the number of trials would rise to 5000 per session, which becomes unfeasible.

In terms of the question of whether humans can detect single photons, it is interesting to compare our approach with the approach followed in [8] using a heralded single-photon source based on SPDC. In that work, approximately 30,000 trials are performed, of which about 2500 are postselected as single-photon trials. The study resulted in a confidence interval for the single-photon accuracy of 0.020 (with a $p$-value of 0.0545) around $a_1 = 0.516$. This value can be compared to our results, indicating a $\tilde{a}_1^{(1)}$ 0.95-HDI length of around 0.048 (0.044) for 5000 (10,000) trials; see Supplement 1, Section S2.2 for $\bar{N}_{\max} = 4.0$. Performing a single simulation and reconstruction using 30,000 trials ($\bar{N}_{\min} = 1.0$, $\bar{N}_{\max} = 4.0$, $p_1 = 0.05$, $D = 5$, $T = 6000$) we find that the $\tilde{a}_1^{(1)}$ 0.95-HDI length drops to 0.036, which is still significantly above 0.020. This indicates that using an SPDC source yields more precise results for $\tilde{a}_1^{(1)}$. However, it would be interesting to apply detector tomography as described in this study to the data obtained in [8], taking into account all trials, or by other authors.

It should be noted that the data from the proposed experiment are useful not only for determining $\vec{a}$ given $n$ photons are presented to the eye, but also for determining $\vec{a}_{\text{ret}}$, the accuracy that $n$ photons are detected given they are incident on the retina, similar to the work presented in [3]. To this end, one could model the cornea, eye lens, and vitreous body as an absorber with transmission $\eta$ and map $\bar{N} \mapsto \eta \bar{N}$ in Eq. (4). Setting priors on $\eta$ and $\vec{a}_{\text{ret}}$, a reconstruction can be performed using the methods described in this work.

## 9. CONCLUSION

We performed a feasibility study on applying detector tomography to the detection of few-photon number states by the human visual system. The main challenge in such an experiment is that the number of trials is limited. Assuming a light source with Poissonian photon statistics, we simulated a 2AFC experiment and reconstructed the photon number accuracies $\vec{a}$, for which we assumed a simple model. It was found that the reconstruction algorithm can reconstruct $\vec{a}$ well. Repeating simulations, we found the optimum experimental parameters to detect whether single photons are detectable (given our model): performing the experiment using at least three source intensities bounded by a minimum average photon number of 1.0 and a maximum average photon number of 4.0, yields the highest chance of detecting $a_1$ to be different from 0.5. Our results suggest that at least 5000 trials are performed, equally distributed over the source intensities. The noise of the light source is expected not to be problematic for this experiment as long as the standard deviation of the average photon number of the source is less than $0.05\bar{N}_{d,0}$, 5% of the nominal mean photon number per pulse. From this study, we conclude that detector tomography is a feasible technique to study human visual perception.

We note that the techniques explored in this study can be applied in a broader perspective. First, they are not limited by Poissonian statistics, but can in principle be applied using any light source as long as the photon statistics of the light presented to the eye are known. Furthermore, these techniques could possibly also be used to study other human senses, particularly the olfactory and gustatory system (Can humans smell/taste few-molecule states?). As such, quantum detector tomography opens the road to study human perception on the quantum level.

**Funding.** Nederlandse Organisatie voor Wetenschappelijk Onderzoek (401.19.032).

**Disclosures.** The authors declare no conflicts of interest.

**Data availability.** Data underlying the results presented in this paper are not publicly available at this time but may be obtained from the authors upon reasonable request.

**Supplemental document.** See Supplement 1 for supporting content.

## REFERENCES

1. J. Lundeen, A. Feito, H. Coldenstrodt-Ronge, K. Pregnell, C. Silberhorn, T. Ralph, J. Eisert, M. Plenio, and I. Walmsley, "Tomography of quantum detectors," Nat. Phys. **5**, 27–30 (2009).
2. A. Feito, J. Lundeen, H. Coldenstrodt-Ronge, J. Eisert, M. Plenio, and I. Walmsley, "Measuring measurement: theory and practice," New J. Phys. **11**, 093038 (2009).
3. J. Renema, G. Frucci, Z. Zhou, F. Mattioli, A. Gaggero, R. Leoni, M. de Dood, A. Fiore, and M. van Exter, "Modified detector tomography technique applied to a superconducting multiphoton nanodetector," Opt. Express **20**, 2806–2813 (2012).
4. M. Loulakis, G. Blatsios, C. Vrettou, and I. Kominis, "Quantum biometrics with retinal photon counting," Phys. Rev. Appl. **8**, 044012 (2017).
5. S. Hecht, S. Schlaer, and M. Pirenne, "Energy at the threshold of vision," Science **93**, 585–587 (1941).
6. B. Sakitt, "Counting every quantum," J. Physiol. **223**, 131–150 (1972).
7. M. Teich, P. Prucnal, G. Vannucci, M. Breton, and W. McGill, "Multiplication noise in the human visual system at threshold. 1. Quantum fluctuations and minimum detectable energy," J. Opt. Soc. Am. **72**, 419–431 (1982).
8. J. Tinsley, M. Molodtsov, R. Prevedel, D. Wartmann, J. Espigulé-Pons, M. Lauwers, and A. Vaziri, "Direct detection of a single photon by humans," Nat. Commun. **7**, 12172 (2016).
9. H. Barlow, "Retinal and central factors in human vision limited by noise," in *Vertebrate Photoreception*, H. B. Barlow and P. Fatt, eds. (Academic, 1977), Chap. 19.
10. P. E. Hallett, "Quantum efficiency of dark-adapted human vision," J. Opt. Soc. Am. A **4**, 2330–2335 (1987).
11. K. Donner, "Noise and the absolute thresholds of cone and rod vision," Vision Res. **32**, 853–866 (1992).
12. E.-J. Wagenmakers, M. D. Lee, T. Lodewyckx, and G. Iverson, "Bayesian versus frequentist inference," in *Bayesian Evaluation of*

*Informative Hypotheses in Psychology*, H. Hoijtink, I. Klugkist, and P. P. A. Boelen, eds. (Springer, 2008), pp. 181–207.
13. C. Curcio, K. Sloan, R. Kalina, and A. Hendrickson, "Human photoreceptor topography," J. Comp. Neurol. **292**, 497–523 (1990).
14. R. Holmes, M. Victora, R. Wang, and P. Kwiat, "Measuring temporal summation in visual detection with a single-photon source," Vision Res. **140**, 33–43 (2017).
15. G. Fechner, *Elemente der Psychophysik* (Breitkopf und Härtel, 1860), Vol. **2**.
16. F. Kingdom and N. Prins, *Psychophysics, a Practical Introduction*, 2nd ed. (Academic, 2016).
17. Y. Yeshurun, M. Carrasco, and L. Maloney, "Bias and sensitivity in two-interval forced choice procedures: tests of the difference model," Vision Res. **48**, 1837–1851 (2008).
18. M. García-Pérez and R. Alcalá-Quintana, "Interval bias in 2AFC detection tasks: sorting out the artifacts," Atten. Percept. Psychophys. **73**, 2332–2352 (2011).
19. G. Westheimer, "The Maxwellian view," Vision Res. **6**, 669–682 (1966).
20. R Core Team, *R: A Language and Environment for Statistical Computing* (R Foundation for Statistical Computing, 2017).
21. Stan Development Team, "RStan: the R interface to Stan," version 2.21.2, GitHub (2020), https://github.com/stan-dev/rstan/ .
22. J. Kruschke, *Doing Bayesian Data Analysis*, 2nd ed. (Academic, 2015).
23. J. M. Dickey, "The weighted likelihood ratio, linear hypotheses on normal location parameters," Ann. Math. Stat. **42**, 204–223 (1971).
24. R. Kelter, "How to choose between different Bayesian posterior indices for hypothesis testing in practice," arXiv, arXiv:2005.13181 (2020).
25. C. Kooperberg, C. Moler, and J. Dongarra, "logspline: routines for logspline density estimation," R package version 2.1.16 (2020).
26. H. Jeffreys, *Theory of Probability*, 3rd ed. (Oxford University, 1961).
27. A. Dey, A. Zele, B. Feigl, and P. P. Adhikari, "Threshold vision under full-field stimulation: Revisiting the minimum number of quanta necessary to evoke a visual sensation," Vision Res. **180**, 1–10 (2021).
28. H. Schütt, S. Harmeling, J. Macke, and F. Wichmann, "Painfree and accurate Bayesian estimation of psychometric functions for (potentially) overdispersed data," Vision Res. **122**, 105–123 (2016).